Surface-Plasmon, Grating-Mode, and Slab-Mode Resonances in the H- and E-Polarized THz Wave Scattering by a Graphene Strip Grating Embedded into a Dielectric Slab

Tatiana L. Zinenko, *Senior Member, IEEE*, Akira Matsushima, *Senior Member, IEEE*, and Alexander I. Nosich, *Fellow, IEEE*

Abstract—We considered the scattering and absorption of the H and E-polarized plane waves by an infinite flat graphene strip grating placed in a dielectric slab, in the THz range. Accurate numerical treatment was based on the singular integral equations and their projection to specially tailored orthogonal polynomials. The resulting numerical algorithm possessed guaranteed convergence and provided controlled accuracy. Reflectance, transmittance, and absorbance were studied, and the resonances on the surface-plasmon modes, the grating modes, and the slab modes were identified. The grating or lattice modes are caused by the periodicity. Their complex frequencies are extremely close to Rayleigh anomalies and therefore the Q-factors are extraordinarily high, which makes them promising in various applications.

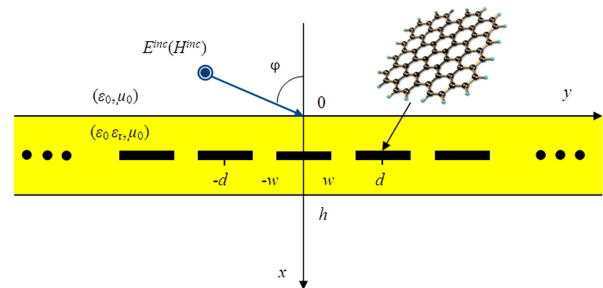*Index Terms*—Graphene strip grating, integral equation, plasmon and grating resonances, scattering.

Fig. 1. Cross-sectional geometry of the plane-wave scattering by a graphene strip grating, embedded in the middle plane of a dielectric slab.

I. INTRODUCTION

WE STUDIED the scattering and absorption of THz waves by an infinite flat grating of graphene strips, embedded into a dielectric slab as depicted in Fig. 1. It is known that the graphene is a few-atom layer of carbon that possesses good electron conductivity that is a function of the frequency, temperature, electron relaxation time and chemical doping [1]. Therefore it can be modeled, even at optical wavelengths, as a zero-thickness imperfect conductor. Worth noting is that this is not possible with many commercial electromagnetic codes, which need introduction of 1 or 2 nm thickness. This leads to numerical inaccuracies and worsens the code performance.

Perhaps the most interesting electromagnetic properties of graphene are found in THz frequency range [2]–[12]. Thanks to the strongly inductive character of graphene's conductivity, it is able to support surface-plasmon waves at the wavelengths two orders of magnitude larger than the noble metals.

The most attractive for applications feature of graphene is the ability to change its conductivity under external electrostatic biasing field, which modifies graphene chemical potential. In practical realization, this can be achieved by placing a layer of metal or semiconductor below the dielectric substrate which supports graphene, and introducing a DC bias.

The patterned graphene, i.e. finite-size structures like strips, disks and more complicated flat shapes offer more degrees of freedom in the design of tunable infrared and THz frequency selective surfaces, plasmonic waveguides, electric switches, sensors, antennas, and absorbers [2]–[7].

Here, the periodic arrays of graphene strips have already attracted great amount of research efforts as promising frequency-selective surfaces and efficient absorbers in the THz frequency range. Infinite gratings of coplanar graphene strips were analyzed by the Fourier expansion method [4], [5] and commercial solver [6], and bad convergence was admitted in the H-case although the surface-plasmon resonances were found and correctly identified in the scattering and absorption.

Still the Fourier method fails to deliver more than a few correct digits as it is divergent in the case of H-polarization, and commercial solvers are also vulnerable for convergence. As we will see further, if a grating is embedded in a thin slab, new extraordinarily high-Q resonances appear. Their trusted modeling makes the use of more sophisticated techniques mandatory. Ac-

$$\begin{cases} (1/2)\left[\vec{E}_T^+(x,y)+\vec{E}_T^-(x,y)\right]=Z\vec{x}\times\left[\vec{H}_T^+(x,y)-\vec{H}_T^-(x,y)\right] \\ \vec{E}_T^+(x,y)=\vec{E}_T^-(x,y), x=h/2, |y-nd|<w,\ n=0,\pm1,\pm2,... \end{cases} \quad (1)$$

curate results serving as reference data were published in [11] and [12] for graphene-strip gratings *in the free space*. These papers worked with singular IEs for the currents on strips; the hyper-type singularity in the H-case was identified as the source of divergence in Fourier-expansion method and commercial solvers. This trouble was overcome with the aid of the Nystrom-type discretization and Chebyshev quadratures in [11] and the method of analytical regularization (MAR) in [12]. In either case the convergence was guaranteed by mathematical theorems; the results were identical.

Unlike [12], our version of MAR technique was a MoM-like treatment based on the projection of relevant IEs on a set of orthogonal polynomials adapted to the edge behavior of the unknown surface current [13]–[15]. This projection combines discretization and regularization in one operation and leads to convergent algorithm, as explained in contributing conference papers [16]–[18]. Here we present briefly this technique and focus on the results of modeling, which we extended to the E-polarization case, and draw deeper conclusions.

In the remainder of the paper, we formulate the scattering problem and briefly present the basic IEs in Section II. Then, in Section III, we explain the essentials of the numerical solution algorithm. Section IV discusses all details of the obtained numerical results. Conclusions are summarized in Section V. Note that we considered time-harmonic waves with the $e^{+j\omega t}$ time dependence, where ω is the cyclic frequency.

II. PROBLEM STATEMENT AND BASIC EQUATIONS

Cross-section of the analyzed scattering problem is shown in Fig. 1. Identical zero-thickness strips had the widths $2w$ and were located in the middle plane of the slab of the thickness h, i.e. at $x = h/2$, with the period d. The incident plane wave propagated in the plane of cross-section of the grating under the angle φ counted from the negative ray of the x axis. The scattered field function had to satisfy the Helmholtz equation and the imperfect-conductor boundary condition imposed on each strip surface [1] - see (1), shown at the top of the page.

Here $Z = 1/\sigma$ is the surface impedance of graphene (i.e. frequency dependent complex-valued resistivity), σ is the surface conductivity, the notations $\pm$ indicate the limiting values at $x \to h/2 \pm 0$, the index T means vectors tangential to the strips, and $\vec{x}$ is the unit vector normal to the strip.

The condition (1) is actually the same as used earlier in the analysis of resistive strip gratings at microwaves [19]–[21]. Still the microwave resistivity of a thinner-than-skindepth metal strip was assumed a real constant while graphene's resistivity in THz range is a complex value (also called surface impedance), strongly dependent on the frequency. In our work, we used the widely accepted model based on the Kubo formulas – see Section IV-D. Note that between 0.1 and 10 THz the intraband conductivity dominates strongly over the interband one.

Besides of (1), other necessary requirements are the edge condition, which limits possible field singularity at the strip edges, and the radiation condition at $x \to \pm\infty$ [13]–[18]. The latter condition means that the field out of the slab with grating must carry the power only away from it.

Under these conditions, the solution to the scattering problem, i.e. the total electromagnetic field, $U = U^{inc} + U^{sc}$, is unique. Here U means E_z or H_z, depending on the polarization, and the incident field is $U^{inc} = e^{-jk_0(x\cos\varphi+y\sin\varphi)}$, where $k_0 = \omega/c$ is the wavenumber and c is the free-space light velocity.

From the Floquet theorem, it follows the quasi-periodicity of the total field: $U(x, y + d) = e^{-j\beta_0 d}U(x, y), \beta_0 = k_0 \sin\varphi$, due to which the scattered field can be expanded as

$$U^{sc}(x,y)=\sum_{l=-\infty}^{\infty}\begin{Bmatrix} \rho_{E,l}\Phi_{E,l}(x), & E-\text{pol} \\ \rho_{H,l}\Phi_{H,l}(x)/j\xi_0, & H-\text{pol} \end{Bmatrix} e^{-j\beta_l y}, \quad (2)$$

where $\rho_{E(H),l}$ are unknown coefficients, $\beta_l = \beta_0 + 2\pi l/d$, and $\Phi_{E(H),l}(x)$ are expressed using the characteristic functions of the dielectric slab (see notations in [14]) and includes Floquet wavenumbers in the free space $\alpha_{0l} = (k_0^2 - \beta_l^2)^{1/2}$ and in the slab $\alpha_{1l} = (\varepsilon_r k_0^2 - \beta_l^2)^{1/2}$. Besides, from the radiation condition it follows that either Re $\alpha_{0l} \geq 0$ or Im $\alpha_{0l} \leq 0$.

On introducing the function $\vec{J}^c(y)$, which stands for the current density, we can write the first of equations (1) as $\vec{E}_T(x, y) = Z\vec{J}^c(y)$. To satisfy the Helmholtz equation, the second of (1), and the radiation condition, U^{sc} can be sought as a double (in H-case) or a single-layer (in E-case) potential. In either case the unknown density function of such potential is the surface current $\vec{J}^c(y)$, which can be expanded into Fourier-Floquet series like (2).

Substituting them the into the first of (1), we arrive at IE,

$$(Z/\zeta_0)F_W(s)+\int_{-1}^{1}K_W(s,t)F_W(t)dt=G_w \quad (3)$$

where $\zeta_0 = \sqrt{\mu_0/\varepsilon_0}$ is the free space impedance, $W = E, H$. The unknown functions $F_W(t)$, the driving functions G_W, and the kernel functions $K_W(s, t)$ are expressed as follows:

$$\begin{bmatrix} F_E(s) \\ F_H(s) \end{bmatrix} = \zeta_0 \begin{bmatrix} J_z^c(y) \\ J_y^c(y) \end{bmatrix} e^{j\beta_0 y}, \begin{bmatrix} G_E \\ G_H \end{bmatrix}$$

$$= \begin{bmatrix} E_z^{\text{pr}}(x_p,y) \\ E_y^{\text{pr}}(x_p,y) \end{bmatrix} e^{-j\beta_0 y}, \quad (4)$$

$$\begin{Bmatrix} K_E(s,t) \\ K_H(s,t) \end{Bmatrix} = \frac{j}{2}\sum_{l=-\infty(even)}^{\infty}$$

$$\begin{Bmatrix} (k_0 w/\pi)\chi_{E,l}\Gamma_{E,l/2} \\ \Delta(\varepsilon_r k_0 d)^{-1}\chi_{H,l}\Gamma_{H,l/2} \end{Bmatrix} e^{jl(t-s)\Delta}, \quad (5)$$

Here $y = ws$, $y' = wt$ and $\Delta = \pi w/d$. Functions $E_{y,z}^{\text{pr}}$ denote the primary field in the absence of the strips (with slab present), and functions $\chi_{E(H),l}$ and $\Gamma_{E(H),l/2}$ are expressed using the characteristic functions of the dielectric slab with the thickness h. These and other notations can be found in [14].

III. REGULARIZING MOMENT-METHOD ALGORITHM

Taking account of the surface-current edge behavior as $J_z^c = \mathrm{O}(1)$ and $J_y^c = \mathrm{O}(r^{1/2})$ if the distance to the edge $r \rightarrow 0$ (see [22]), we project each current to the set of orthogonal polynomials as basis functions, $F_E(t) = \sum_{n=0}^{\infty} f_{E,n} P_n(t)$ and $F_H(t) = \sqrt{1-t^2} \sum_{n=1}^{\infty} f_{H,n} U_{n-1}(t)$, in the E- and H-cases, which are the Legendre polynomials and the Chebyshev polynomials of the second kind, respectively. They are further used as a full-wave Galerkin basis to discretize IE (3). Hence, we multiply both sides of (3) with $P_m(s)$ (in E-case) or $U_{m-1}(s)\sqrt{1-s^2}$ (in H-case) and integrate it from -1 to 1 with respect to s. This projection brings us to the following two infinite matrix equations, where $m = 0, 1, 2, ...$ and $m = 1, 2, 3, ...$, respectively:

$$\sum_{n=0}^{\infty} (\delta_{mn} + \kappa_{E,mn}) f_{E,n} = \zeta_0/ZG_E(2m+1)\delta_{m0}, \quad (6)$$

$$\sum_{n=1}^{\infty} (\delta_{mn} + \kappa_{H,mn}) f_{H,n} = \pi\tilde{w}(2n)^{-1} G_H \delta_{m1}, \quad (7)$$

$$\kappa_{E,mn} = \frac{\zeta_0 k_0 w}{\pi Z}(2m+1)j^{n-m+1}$$
$$\times \sum_{\substack{l=-\infty \\ (even)}}^{+\infty} \chi_{E,l}\Gamma_{E,l/2}j_m(l\Delta)j_n(l\Delta) \quad (8)$$

$$\kappa_{H,mn} = \frac{Z\tilde{w}}{\zeta_0 n}\tilde{\kappa}_{H,mn} - \frac{\Delta^2\tilde{\chi}_{H,0}}{2n}\delta_{m1}\delta_{n1} - 2mj^{n-m}$$
$$\times \sum_{\substack{l=-\infty \\ (l\neq 0)}}^{+\infty} \tilde{\chi}_{H,l}\frac{J_m(l\Delta)J_n(l\Delta)}{l^2} \quad (9)$$

$\tilde{\kappa}_{H,mn} = 0$ if $m+n$ is odd or $[1-(m-n)^2]^{-1} - [1-(m+n)^2]^{-1}$ if otherwise, $\tilde{w} = j4k_0 w\varepsilon_r/\pi$, δ_{mn} is Kronecker's delta, and J_m and j_m are usual and spherical Bessel functions, respectively. As the property $\sum_{n,m=0(1)}^{+\infty} |\kappa_{E(H),mn}|^2 < \infty$ holds, then (6) and (7) are the Fredholm second-kind matrix equations [23]. This guarantees the convergence of numerical results when (6) or (7) is truncated to finite order (the internal sums are convergent and must be calculated with a superior accuracy).

IV. RESONANCES AND NEAR FIELD PORTRAITS

First of all, we present in Figs. 2 and 3 the frequency scans, in the THz range, of the transmittance (T), reflectance (R) and absorbance (A) in terms of power for the graphene-strip grating suspended in the free space (dashed lines) and embedded into a dielectric slab (solid line).
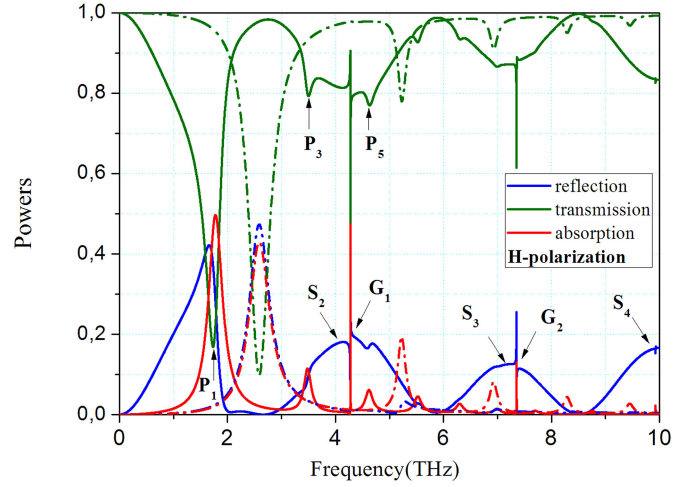

Fig. 2. The frequency spectra of the transmittance, reflectance, and absorbance for one-layer graphene strip grating with the strip width $2w = 20\,\mu\text{m}$ and the period $d = 70\,\mu\text{m}$ embedded in the dielectric slab with $\varepsilon_r = 2.25$ and $h/d = 0.5$ (solid curves) and in free space (dashed curves) under the normal incidence ($\varphi = 0^o$) of the unit-amplitude H-polarized plane wave. Graphene parameters are $\tau = 1\,\text{ps}$, $\mu_c = 0.39\,\text{eV}$ and T = 300 K. Resonances on the natural modes are marked with arrows.
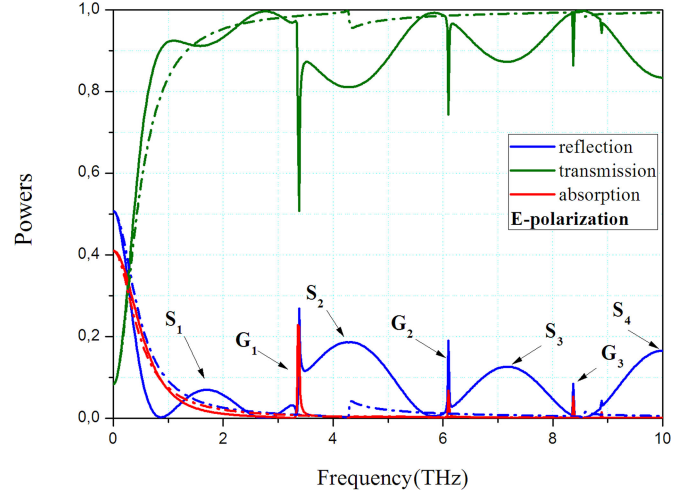

Fig. 3. The same as in Fig. 2 however for the E-polarization case.

The grating is illuminated by the normally incident H and E-polarized plane waves of unit amplitude, respectively. To calculate the frequency-dependent surface impedance of graphene, we used the Kubo formulas (see Section IV-D).

The truncation orders of the matrix equations (6) and (7) and those of the corresponding Floquet series expansions of the field components and surface currents were adapted to provide 5-digit or better accuracy of computations.

A. H-Polarization Case

In this case the E-field vector lies in the cross-sectional plane of the grating that is necessary condition to observe the surface-plasmon resonances. Indeed, in Fig. 2 one can see intensive resonances denoted as P_1, P_3, and P_5, which are the resonances on the surface-plasmon modes excited on every strip. They are
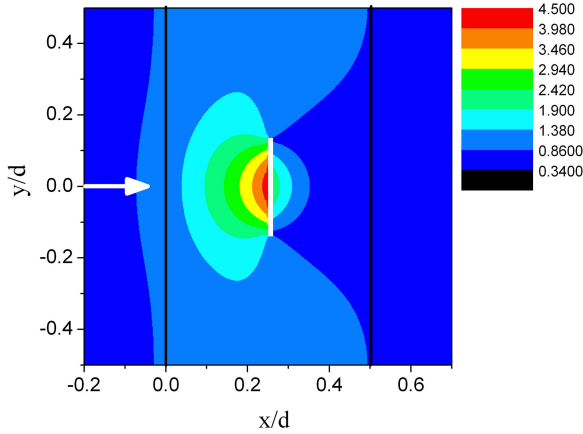
Fig. 4. Near field pattern in the plasmon resonance P_1 at $f = 1.77742$ THz at a single period. The strip is shown as a white box, and slab's boundaries are given by black lines. Other parameters are the same as in Fig. 2.
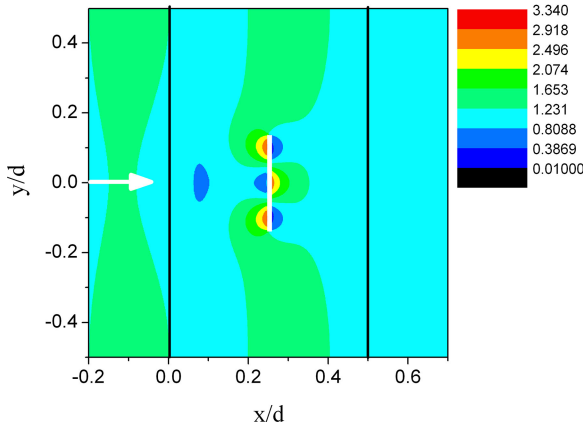

Fig. 5. Near field pattern in the plasmon resonance P_3 at $f = 3.481960$ THz. Other parameters are the same as in Fig. 2.

best visible on the absorption spectrum as the slab is assumed lossless; the most intensive is the lowest in frequency resonance on the mode P_1 around 1.8 THz. This is almost exactly $\varepsilon_r^{-1/2}$ times the corresponding frequency, 2.7 THz, of the free space case.

The nature of these modes can be understood if one considers them as Fabry-Perot standing waves formed by the surface-plasmon natural wave of a graphene layer bouncing between the strip edges [24], [25]. This is supported by Figs. 4–6 showing the near-field portraits of the absolute value of the magnetic field. The normalized propagation constant of that wave, γ_{plas}, is found analytically using the condition (1),

$$\gamma_{plas} = [1 - (2/\sigma\zeta_0)^2]^{1/2} \qquad (10)$$

The corresponding approximate characteristic equation is

$$\sin(\mathrm{Re}\gamma_{plas}2\tilde{k}w) = \sin\left(\mathrm{Re}[1 - (2/\sigma\zeta_0)^2]^{1/2}2\tilde{k}w\right) \approx 0, \qquad (11)$$

where $\tilde{k}$ is k_0 for the grating in free space and $k_0\varepsilon_r^{1/2}$ in a slab.

The roots of (11) determine the natural frequencies of the plasmon modes whose fields are symmetric and antisymmetric
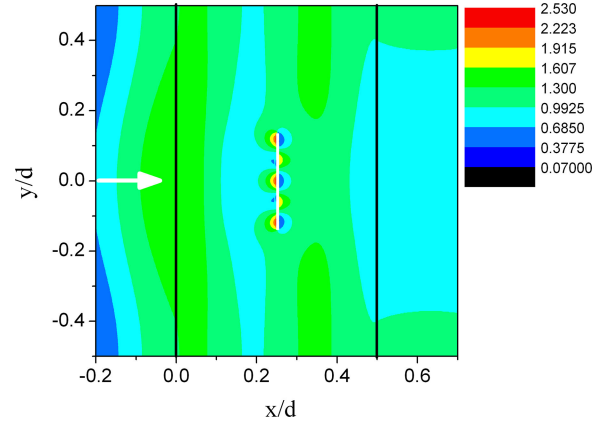

Fig. 6. Near field pattern in the plasmon resonance P_5 at $f = 4.621172$ THz. Other parameters are the same as in Fig. 2.

with respect to the strip middle point. Their indices are odd ($n = 1, 3, \ldots$) or even ($n = 2, 4, \ldots$) numbers, respectively, and then the approximate resonance condition is

$$f_n^{(P)} \approx cn/(4w\varepsilon_r^{1/2}\,\mathrm{Re}\gamma_{plasm}). \qquad (12)$$

More details on the approximate analysis of the single graphene strip resonances P_n and their sensitivities to the changes of host medium bulk refractive index can be found in [25], [26]. In the THz range, the Q-factors of plasmon modes on graphene microstrip have medium values, $Q_n^{(P)} \approx 10 \div 100$.

As the plots in Fig. 2 correspond to the case of the normal incidence, only the odd-index surface-plasmon resonances are excited. This is because the incident wave is symmetric relatively to the strip middle point while the natural fields of the even-index modes are anti-symmetric relatively to that point and hence their excitation needs inclined incidence.

Besides of them, in the presence of a dielectric slab one can see much sharper spikes on the so-called grating (a.k.a. lattice) modes G_1, G_2 and G_3, predicted in [27] (they exist even if strips are PEC [28]). For experimental observation of them in the visible range on arrays of metal particles, see [29]. Under the normal incidence, the grating modes have the frequencies controlled by the period and the slab parameters. Namely, they are shifted from the free-space Rayleigh anomalies by the frequency-dependent factor γ_0^H ($1 < \gamma_0^H < \varepsilon_r^{1/2}$)

$$f_n^{(GH)} \approx cn/(d\gamma_0^H) \qquad (13)$$

The value γ_0^H is the normalized propagation wavenumber of the principal H-type guided mode of the dielectric slab. Thus, if the slab thickness or contrast gets larger (or smaller), the grating-mode frequencies tend to the Rayleigh anomalies of the slab material (or of the free space) and eventually vanish there if the host medium becomes homogeneous.

Note that the near-field portraits in the grating resonances, shown in Figs. 7 and 8, are drastically different from the field portraits in the plasmon resonances (compare to Figs. 4–6). Instead of sticking to the strips, the field hot spots form extended shapes across the whole slab cross-section and even stretching far away from the slab to the free space. This field pattern is caused by the periodicity as explained in review [27];
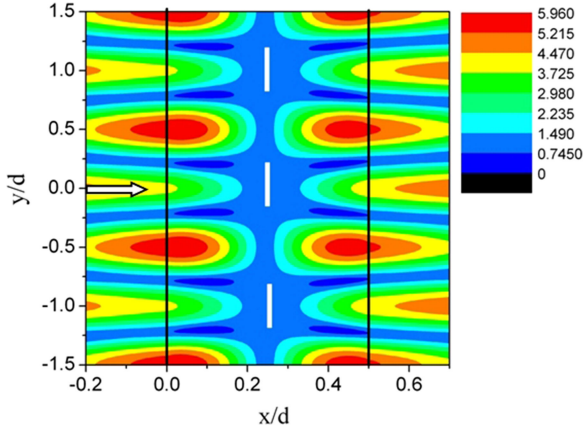
Fig. 7. Near field pattern in the grating resonance $G_{H,1}$ at $f = 4.27427$ THz at three periods of grating. Other parameters are the same as in Fig. 2.
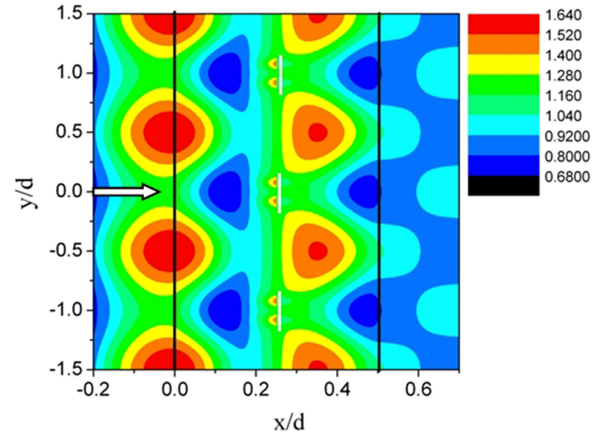

Fig. 9. Near field pattern in the slab resonance $S_{H,2}$ at $f = 4.148$ THz at three periods of grating. Other parameters are the same as in Figs. 2–7.
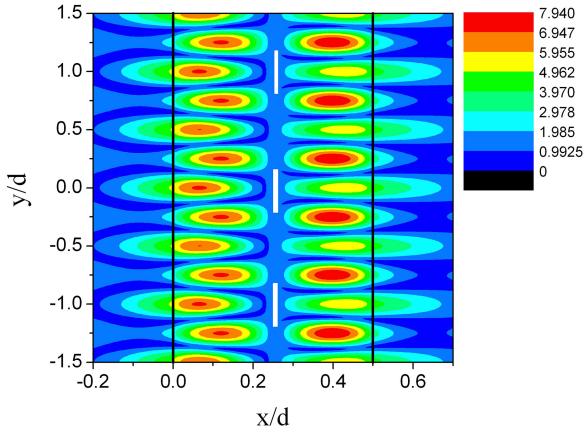

Fig. 8. Near field pattern in the grating resonance $G_{H,2}$ at $f = 7.353566$ THz. Other parameters are the same as in Figs. 2–6.
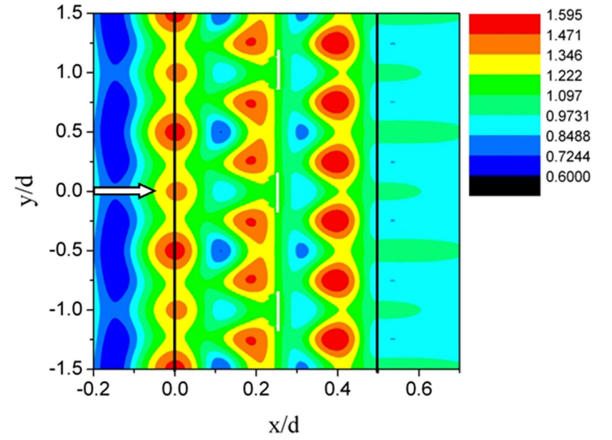

Fig 10. Near field pattern in the slab resonance $S_{H,3}$ at $f = 7.2$ THz. Other parameters are the same as in Figs. 2–8.

note that direct relatives of the grating-mode resonances are the Bragg resonances in the scattering by finite periodic scatterers. If the slab is lossless, their Q-factors are controlled by the slab thickness mainly, $Q_n^{(GH)} = O(d^8/h^8)$, so that in our example $Q_n^{(GH)} \approx 100 \div 1000$.

Finally, additional family of low-Q resonances can be seen that appears only for a grating embedded into a slab. Close inspection shows that their frequencies are dependent mainly on the slab thickness and its dielectric constant,

$$f_n^{(S)} \approx cn/(h\varepsilon_r^{1/2}) \qquad (14)$$

and their Q-factors are low, $Q_n^{(S)} \approx 1 \div 10$. These are the resonances on the modes of the bare dielectric slab as a Fabry-Perot etalon, $S_{2,3,4}$, slightly perturbed by the presence of the grating. Their near-field portraits are presented in Figs. 9–11. Note that the lowest resonance of that type, S_1, is fully overshadowed by the higher-Q plasmon resonance P_1.

B. E-Polarization Case

In the *E*-polarization case, the THz-range transmittance, reflectance and absorbance of the same graphene-strip grating
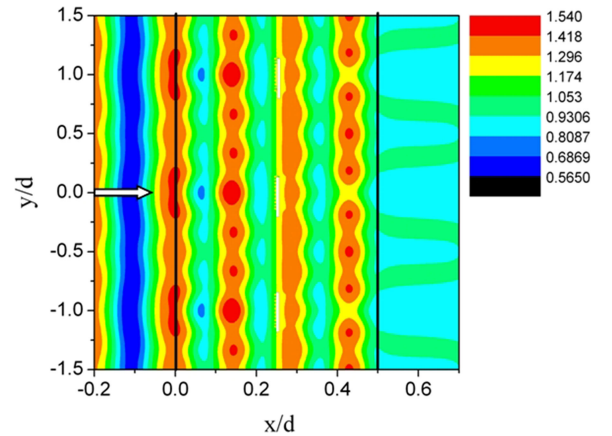

Fig. 11. Near field pattern in the slab resonance $S_{H,4}$ at $f = 10$ THz. Other parameters are the same as in Figs. 2–9.

embedded into a dielectric layer are shown in Fig. 3. Here, the E-field vector was parallel to the strips, in which case a sheet of graphene cannot support surface-plasmon waves. Thus, the frequency dependences of *T*, *R* and *A* for a suspended grating of strips (dashed curves) do not display any resonances. Only the $\pm 1 - $ st and $\pm 2 - $ nd Rayleigh anomalies at 4.2 and 8.4 THz
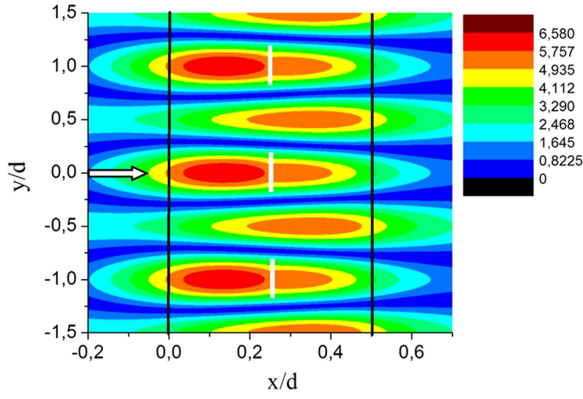
Fig. 12. Near field pattern in the grating resonance $G_{E,1}$ at $f = 3.3834576$ THz. Other parameters are the same as in Fig. 2.
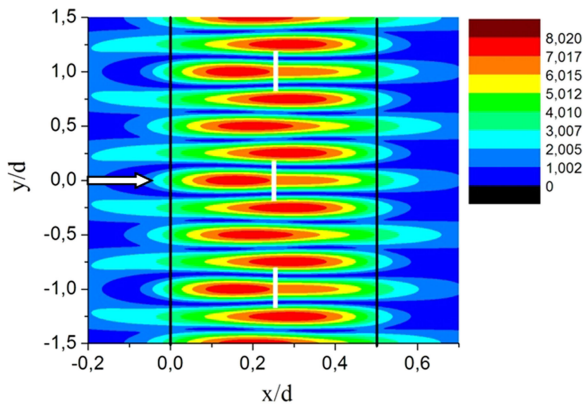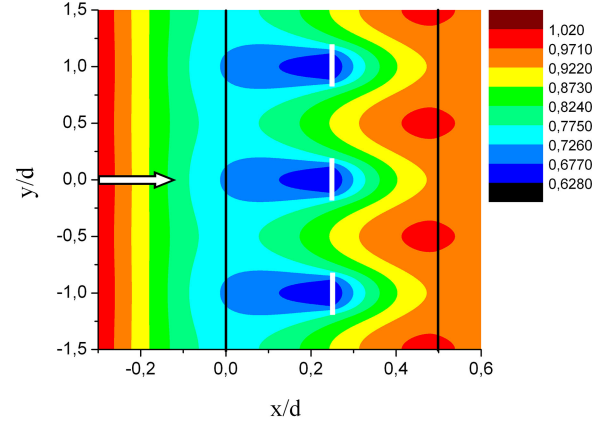

Fig. 14. Near-field pattern in the slab resonance $S_{E,1}$ at $f = 1.606$ THz. Other parameters are the same as in Fig. 2.

Fig. 13. Near field pattern in the grating resonance $G_{E,2}$ at $f = 6.103$ THz. Other parameters are the same as in Fig. 2.
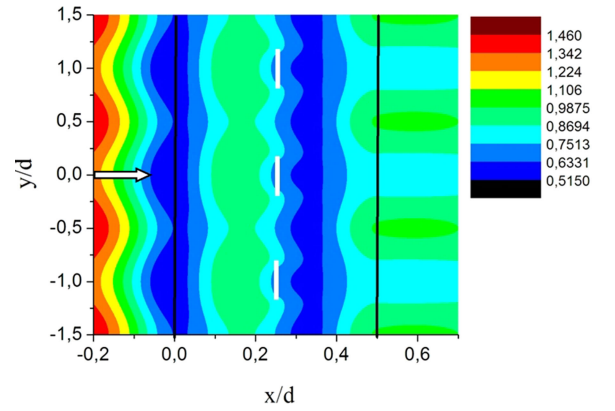
Fig. 15. Near field pattern in the slab resonance $S_{E,2}$ at $f = 4.3042$ THz. Other parameters are the same as in Fig. 2.

are seen as sharp bends of the plots at the wavelengths being entire divisions of the period (here the derivatives of the curves of T, R and A in frequency loose continuity).

In contrast, for the grating embedded into the slab, the resonances on the grating modes G_1, G_2, and G_3 appear. Their frequencies are given by approximate formula like (13) where one has to replace γ_0^H with the similar quantity γ_0^E for the principal E-type guided mode of the dielectric slab. They are more shifted from the free-space Rayleigh anomalies because $1 < \gamma_0^H < \gamma_0^E < \varepsilon_r^{1/2}$ at any frequency. Note that their Q-factors are superior over the other resonances, although they are less sharp than in the H-polarization case. The near-zone E-field patterns in the grating-mode resonances are shown in Figs. 12 and 13 and demonstrate the same features as in H-case.

Besides, low-Q resonances on the dielectric slab modes $S_{1,2,3,4}$ appear at the frequencies (14) (identical for both polarizations at the normal incidence), which depend on slab's thickness and dielectric constant (see Figs. 14–16).

C. Polarization Discrimination

As one can see, the position of the first plasmon resonance P_1 depends on the strip width. At the lower frequencies, say

Fig. 16. Near field pattern in the slab resonance $S_{E,3}$ at $f = 7.174$ THz. Other parameters are the same as in Fig. 2.

below 0.5 THz for the strip width $2w = 20\,\mu$m (exact value depends on μ_c and ε_r), a graphene-strip grating embedded into a slab displays rather good polarization discrimination in usual sense. This is traditional Hertz effect: H-wave is transmitted and E-wave is reflected (although absorption is significant).

(a)

(b)

Fig. 17. Color maps (reliefs) of the reflectance as a function of the frequency and the relative permittivity of the dielectric slab in the case of H-wave (a) and E-wave (b) incident normally on the grating-in-slab. Parameters of the slab and the graphene-strip grating are the same as in Figs. 2–16.
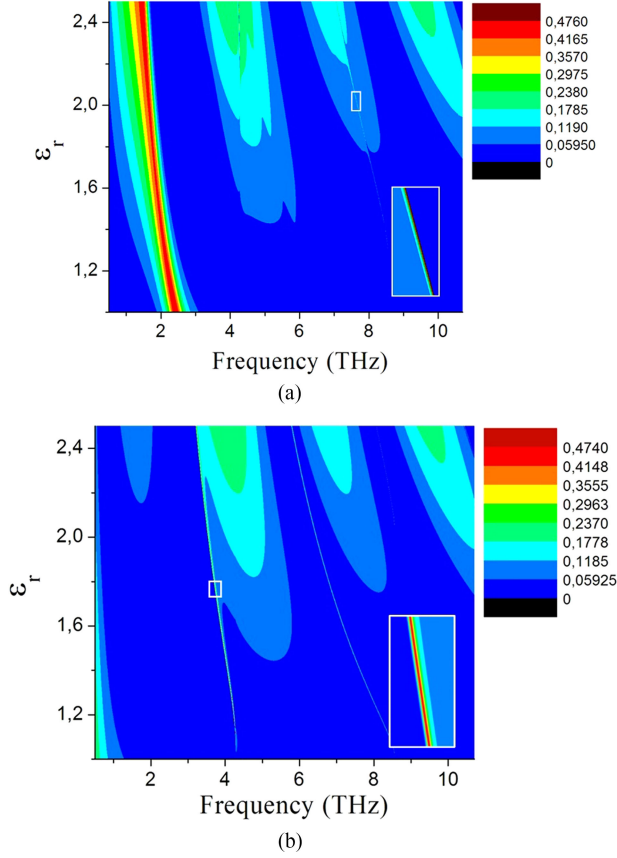
Still note that the first plasmon mode P_1 destroys the Hertz effect and actually creates the opposite situation: at the first-plasmon frequency, *E*-wave is transmitted and *H*-wave is reflected although its absorption is comparable to reflection. The latter effect can be potentially used in the design of *tunable* polarizers in applications not very critical to losses.

These considerations are even better understandable if the reflectance is presented as a color map of the function of two variables, frequency and, say, slab's dielectric permittivity. Such maps, for two polarizations, are shown in Fig. 17. Here the bright red "ridges" correspond to high reflectance; they stretch according to the approximate formulas (12)–(14). The insets demonstrate the details of the resonances on the grating modes, which make so narrow and sharp ridges that they are hardly resolved without a 10-fold zoom.

D. Role of Electron Relaxation Time

The authors of [30] attracted our attention to the role of the electron relaxation time in the THz response of the patterned graphene. According to them, the value of 1 ps is on the higher edge of realistic variation domain. Therefore we studied the effect of τ on the resonance effects.
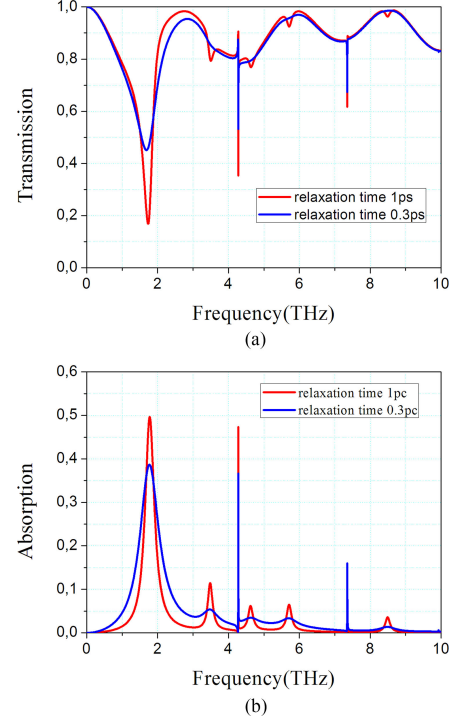

(a)

(b)

Fig. 18. The frequency dependences of the transmittance (a) and absorbance (b) for a flat graphene strip grating with the strip width $2w = 20\,\mu$m and the period $d = 70\,\mu$m embedded into a dielectric slab with $\varepsilon_r = 2.25$ and $h/d = 0.5$ under the normal incidence ($\varphi = 0^o$) of the unit-amplitude *H*-polarized plane wave. Graphene parameters are $\mu = 0.39\,$eV and $T = 300\,$K.

Note that the Kubo description tells that graphene's conductance is a sum of the intraband and interband terms,

$$\sigma(\omega,\mu_c,\tau,T) = \sigma_{\mathrm{intra}}(\omega,\mu_c,\ \tau,T) + \sigma_{\mathrm{inter}}(\omega,\mu_c,\tau,T). \tag{15}$$

In the THz range, two terms of (15) can be simplified and cast to the following form [25]:

$$\sigma_{\mathrm{intra}} = \frac{-jq_e^2 k_B T}{\pi\hbar^2(\omega - j\tau^{-1})}\left(\frac{\mu_c}{k_B T} + 2\ln\left[1+\exp\left(-\frac{\mu_c}{k_B T}\right)\right]\right),$$

(here, some misprints)

$$\tag{16}$$

$$\sigma_{\mathrm{inter}} \simeq \frac{-jq_e^2 k_B T}{4\pi\hbar^2}\left(\frac{2|\mu_c| - (\omega - j\tau^{-1})\hbar}{2|\mu_c| + (\omega - j\tau^{-1})\hbar}\right), \tag{17}$$

where q_e is the elementary charge, $\hbar$ is the reduced Plank constant, and k_B is the Boltzmann constant. Slightly different approximate expressions for these values can be found in literature, e.g. in [1]; still they yield similar numerical results.

In the THz range, the intraband conductivity (16) is 1–2 orders larger than the interband one (17). As one can see from (16), the electron relaxation time is responsible for $\mathrm{Re}\sigma_{intra}$. Hence, the value of τ should influence the surface-plasmon modes P_n excited on each strip of the grating.

In Fig. 18, we presented T and A scans for a grating-in-slab in the THz range, computed for $\tau = 1$ ps and $\tau = 0.3$ ps. As expected, such reduction of electron relaxation time led to the 30% drop of the P_1 dip. All higher-order low-Q resonances $P_{3,5,7,9}$ got spoiled and remained visible only in the absorption.

In contrast, the sharp resonances on high-Q grating modes were only slightly affected by the smaller relaxation time. This was apparently because they were caused by the periodicity. The low-Q resonances in T on the slab modes (absent for A) were intact, especially in the higher THz range.

V. CONCLUSION

We presented results of the accurate numerical analysis, using the IE-based method, of the scattering and absorption of THz waves by a graphene-strip grating embedded into a lossless dielectric slab. Both the E- and H-polarization cases were considered and revealed the potentialities of the discrimination between two polarizations.

Besides of the resonances on the surface-plasmon modes known in the H-polarization, we quantified, apparently for the first time, the resonances on the grating modes and the slab modes. Note than the grating-mode resonances do not appear on a graphene-strip grating suspended in the free space ([1], [11], [12]). However they exist on such grating in any thin dielectric slab and possess far superior Q-factors. In the E-polarization case, plasmons are absent however both the grating-mode and the slab-mode resonances are present. These results can be useful in the development of novel tunable filters, sensors, absorbers and polarizers incorporating periodically patterned graphene.

We would like to emphasize that although the resonances on the grating modes can be apparently found with less advanced numerical methods, such as Fourier method, and with rough commercial codes, the use of more accurate techniques is mandatory. This is because Q-factors of the grating modes become extraordinarily high (10^6 and higher) if the dielectric slab is moderately thin, say, 1 μm. It means that 6 and more correct digits in the numerical solution should be delivered, that is beyond the capabilities of the mentioned non-convergent methods. In contrast, the presented advanced algorithm can easily perform such analysis; moreover, it can serve as a core of efficient numerical optimization code in the computer-aided design of such devices.

REFERENCES

[1] R. Depine, *Graphene Optics: Electromagnetic Solution of Canonical Problems,* IOP Concise Physics. San Raefel, CA, USA: Morgan & Claypool Publishers, 2016.

[2] R. Filter *et al.*, "Tunable graphene antennas for selective enhancement of THz emission," *Opt. Exp.*, vol. 21, pp. 3737–3745, 2013.

[3] S. Thongrattanasiri, F. H. L. Koppens, and F. J. Garcia de Abajo, "Complete optical absorption in periodically patterned graphene," *Phys. Rev. Lett.*, vol. 108, pp. 047401–047405, 2012.

[4] A. Y. Nikitin, F. Guinea, F. J. Garcia-Vidal, and L. Martin-Moreno, "Surface plasmon enhanced absorption and suppressed transmission in periodic arrays of graphene ribbons," *Phys. Rev. B*, vol. 85, p. 081405(R)/4, 2012.

[5] A. Khavasi, "Fast convergent Fourier modal method for the analysis of periodic arrays of graphene ribbons," *Opt. Lett.*, vol. 38, no. 16, pp. 3009–3012, 2013.

[6] B. Vasic, G. Isic, and R. Gajic, "Localized surface plasmon resonances in graphene ribbon arrays for sensing of dielectric environment at infrared frequencies," *J. Appl. Phys.*, vol. 113, no. 1, p. 113110/7, 2013.

[7] K. R. Jha and G. Singh, "Terahertz planar antennas for future wireless communication: A technical review," *Infrared Phys. Technol.*, vol. 60, pp. 71–80, 2013.

[8] R. Yu, R. Alaee, F. Lederer, and C. Rocksruhl, "Manipulating the interaction between localized and delocalized surface plasmon-polaritons in graphene," *Phys. Rev. B*, vol. 90, p. 085409/10, 2014.

[9] R.-B. Hwang, "Rigorous formulation of the scattering of plane waves by 2-D graphene-based gratings: Out-of-plane incidence," *IEEE Trans. Antennas Propag.*, vol. 62, no. 9, pp. 4736–4745, Sep. 2014.

[10] Z. Xu, X. Dong, and J. Bornemann, "Design of a reconfigurable MIMO system for THz communications based on graphene antennas," *IEEE Trans. THz Sci. Technol.*, vol. 4, no. 5, pp. 609–617, Sep. 2014.

[11] O. V. Shapoval *et al.*, "Integral equation analysis of plane wave scattering by coplanar graphene-strip gratings in the THz range," *IEEE Trans. THz Sci. Technol.*, vol. 3, no. 5, pp. 666–673, 2013.

[12] T. L. Zinenko, "Scattering and absorption of terahertz waves by a free-standing infinite grating of graphene strips: Analytical regularization analysis," *IOP J. Opt.*, vol. 17, no. 5, p. 055604/8, 2014.

[13] A. Matsushima, T. L. Zinenko, H. Minami, and Y. Okuno, "Integral equation analysis of plane wave scattering from multilayered resistive strip gratings," *J. Electromagn. Waves Appl.*, vol. 12, pp. 1449–1469, 1998.

[14] T. L. Zinenko, A. Matsushima, and Y. Okuno, "Scattering and absorption of electromagnetic plane waves by a multilayered resistive strip grating embedded in a dielectric slab," *Trans. IEICE Electron.*, vol. E82-C, no. 12, pp. 2255–2264, 1999.

[15] A. Matsushima, T. L. Zinenko, H. Nishimori, and Y. Okuno, "Plane wave scattering from perpendicularly crossed multilayered strip gratings," *Progress Electromagn. Res.*, vol. 28, pp. 189–207, 2000.

[16] T. L. Zinenko, A. Matsushima, and A. I. Nosich, "Integral equations and sophisticated moment method in the scattering of the terahertz plane waves of two polarizations by a grating of graphene strips," in *Proc. Int. Conf. Microwaves (MIKON-2014)*, Gdansk, Poland, 2014, pp. 545–548.

[17] T. L. Zinenko, A. Matsushima, and A. I. Nosich, "Frequency and polarization selectivity of graphene strip gratings," in *Proc. Eur. Microw. Conf.*, Paris, France, 2015, pp. 191–194.

[18] T. L. Zinenko, A. Matsushima, and A. I. Nosich, "Identification of H-type resonances on a flat graphene strip grating in a dielectric slab," in *Proc. Eur. Conf. Antennas Propag.*, Davos, Switzerland, 2016, pp. 1–4.

[19] R. C. Hall and R. Mittra, "Scattering from a periodic array of resistive strips," *IEEE Trans. Antennas Propag.*, vol. AP-33, no. 9, pp. 1009–1011, Sep. 1985.

[20] R. Orta, P. Savi, and R. Tascone, "The effect of finite conductivity on frequency selective surface behavior," *Electromagn.*, vol. 10, no. 2, pp. 213–227, 1990.

[21] T. L. Zinenko, A. I. Nosich, and Y. Okuno, "Plane wave scattering and absorption by resistive-strip and dielectric-strip periodic gratings," *IEEE Trans. Antennas Propag.*, vol. 46, no. 10, pp. 1498–1505, Oct. 1998.

[22] I. M. Braver, P. S. Fridberg, K. L. Garb, and I. M. Yakover, "The behavior of the electromagnetic field near the edge of a resistive half-plane," *IEEE Trans. Antennas Propag.*, vol. 36, no. 12, pp. 1760–1768, Dec. 1988.

[23] A. I. Nosich, "Method of analytical regularization in computational photonics," *Radio Sci.*, vol. 51, no. 8, pp. 1421–1430, 2016.

[24] M. V. Balaban, O. V. Shapoval, and A. I. Nosich, "THz wave scattering by a graphene strip and a disk in the free space: integral equation analysis and surface plasmon resonances," *IOP J. Opt.*, vol. 15, no. 11, p. 114007/8, 2013.

[25] O. V. Shapoval and A. I. Nosich, "Bulk refractive-index sensitivities of the THz-range plasmon resonances on a micro-size graphene strip," *IOP J. Phys. D: Appl. Phys.*, vol. 49, no. 5, p. 055105/8, 2016.

[26] A. P. Anyutin, I. P. Korshunov, and A. D. Shatrov, "Quasi-static plasmon resonances in a graphene ribbon in the infrared range," *J. Commun. Technol. Electron.*, vol. 61, no. 6, pp. 607–613, 2016.

[27] V. O. Byelobrov, T. L. Zinenko, K. Kobayashi, and A. I. Nosich, "Periodicity matters: grating or lattice resonances in the scattering by sparse arrays of sub-wavelength strips and wares," *IEEE Antennas Propag. Mag.*, vol. 57, no. 6, pp. 34–45, Dec. 2015.

[28] R. Rodríguez-Berral, F. Medina, F. Mesa, and M. García-Vigueras, "Quasi-analytical modeling of transmission/reflection in strip/slit gratings loaded with dielectric slabs," *IEEE Trans. Microw. Theory Techn.*, vol. 60, no. 3, pp. 405–418, Mar. 2012.

[29] M. B. Ross, C. A. Mirkin, and G. C. Schatz, "Optical properties of one-, two-, and three-dimensional arrays of plasmonic nanostructures," *J. Phys. Chem. C*, vol. 120, pp. 816–830, 2016.

[30] S. M. Kukhtaruk and V. A. Kochelap, "Semiclassical analysis of intraband collective excitations in a two-dimensional electron gas with Dirac spectrum," *Phys. Rev. B*, vol. 92, no. 4, p. 041409/5(R), 2015.

Tatiana L. Zinenko (M'00–SM'14) was born in Alchevsk, Ukraine. She received the M.S. degree in radio physics from the Kharkiv National University, Kharkiv, Ukraine, the D.E. degree in system science from the Kumamoto University, Kumamoto, Japan, in 2000, and the Ph.D. degree in radio physics from Institute of Radio Physics and Electronics of the National Academy of Sciences of Ukraine (IRE NASU), Kharkov, Ukraine, in 2004. She joined the IRE NASU, where she is currently a Senior Scientist and the acting Head of the Department of Quasi-Optics. From 1996 to 2000, she was in the Department of Computer and Electrical Engineering, Kumamoto University, Kumamoto, Japan, as a Research Student. Her research interests are in integral equation methods and electromagnetic wave scattering from imperfect scatterers and periodic gratings. In 1999, she received the SUMMA Graduate Student Fellowship in advanced electromagnetics.

Akira Matsushima (M'08–SM'10) was born in 1958 in Kumamoto, Japan. He received the B.E. degree in electrical engineering from the Kumamoto University, Kumamoto, Japan, in 1980, and the M.E. and D.E. degrees in computational electromagnetics from the Kyushu University, Fukuoka, Japan, in 1982 and 1994, respectively. He joined Kumamoto University in 1982 as a Research Associate, and is currently a Professor at the Faculty of Advanced Science and Technology. He is currently working in the area of numerical methods for electromagnetic boundary value problems based on integral equations and mode expansions.

Alexander I. Nosich (M'94–SM'95–F'04) was born in 1953 in Kharkiv, Ukraine. He received the M.S., Ph.D., and D.Sc. (higher doctorate) degrees in radio physics from the Kharkiv National University, Ukraine, in 1975, 1979, and 1990, respectively.

Since 1979, he has been in the Institute of Radio Physics and Electronics of the National Academy of Science of Ukraine, Kharkiv, Ukraine, where he is currently a Professor and Principal Scientist heading the Laboratory of Micro and Nano Optics. Since 1992, he has held a number of guest fellowships and professorships in the EU, Japan, Singapore, and Turkey. His research interests include the method of analytical regularization, propagation and scattering of waves, open waveguides, antennas, and lasers. Dr. Nosich was one of the initiators and technical committee Chairman of the international conference series on Mathematical Methods in Electromagnetic Theory. In 1995, he organized the IEEE AP-S East Ukraine Chapter, the first one in the former USSR. He currently represents Ukraine and Georgia in the European Association on Antennas and Propagation.